1 # **Supplementary files**

2 Insight into the potential application of CuO_x/CeO_2 catalyst for NO removal by CO:

3 perspective from the morphology & crystal-plane of CeO_2

4 Yali Du [a,1], Dong Lu [b,1], Jiangning Liu [b], Xiaodong Li [a], Chaohui Wu [b], Xu Wu [b,*], Xia An

5

6 [a] College of Chemistry and Chemical Engineering, Jinzhong University, Jinzhong 030619, China.

7 [b] College of Chemistry and Chemical Engineering, Taiyuan University of Technology, Taiyuan

8 030024, China.

9

10 [1] These authors contributed equally to this work.

11 **Corresponding Authors**

12 * E-mail: wuxu@tyut.edu.cn (Xu Wu)

13

1 Experimental section

1.1 Details of catalytic performance evaluation

S_{BET} normalized reaction rates (rs, mol m^{-2} s^{-1}) was calculated by the following formula:

$$rs\ (mol\ m^{-2}\ s^{-1}) = \frac{C_{in} \times F}{m_{cat} \times S_{BET}} \times \ln(1-X)$$

Where C_{in} refers to the NO concentration (ppm) in the inlet gas, F (mol s^{-1}) is the flow rate, m_{cat} (g) is the mass of catalyst, S_{BET} (m^2 g^{-1}) is the specific surface area calculated via BET method, X is the NO conversion.

1.2 Calculation of turnover frequency (TOF)

TOF value, representing the turnover conversion of single active sites per second, was calculated as following equation:

$$TOF = \frac{v \times a}{V_m \times n_{Cu-surf}}$$

Where v is the flow rate of NO (m^3 s^{-1}), V_m is the gas molar constant (m^3 mol^{-1}), a is the NO conversion at certain temperature (%), $n_{Cu-surf}$ is the mole number of active Cu atoms on the catalytic surface (mol). Notedly, the NO conversion was controlled below 20% within the whole temperature range to avoid the heat transfer effect (The corresponding data were displayed in Fig. S6 and Table S3). $n_{Cu-surf}$ was calculated as following equation:

$$n_{Cu-surf} = \frac{N_{Cu-surf}}{N_A}$$

Where $N_{Cu\text{-}surf}$ is mole number of active Cu atoms on the catalytic surface and N_A is the Avogadro constant (6.02×10^{23} mol^{-1}). Then $N_{Cu\text{-}surf}$ was calculated as following equation:

$$m_{catal} \times S_{surf} = S_{Cu\text{-}surf} + S_{Ce\text{-}surf} + S_{O\text{-}surf}$$

$$= N_{Cu\text{-}surf} \times S_{Cu\text{-}single} + N_{Ce\text{-}surf} \times S_{Ce\text{-}single} + N_{O\text{-}surf} \times S_{O\text{-}single}$$

where m_{catal} (g) is the mass of catalyst, S_{surf} (m^2 g^{-1}) is the surface area of catalysts by BET method, $S_{Cu\text{-}single}$ (m^2), $S_{Ce\text{-}single}$ (m^2), and $S_{O\text{-}single}$ (m^2) are surface area of single atoms, r (m) is the value of atomic radii.

The atomic radii employed for Cu, Ce and O are shown as follows:

$r_{Cu} = 1.28 \times 10^{-10}$ m, $r_{Ce} = 1.83 \times 10^{-10}$ m, $r_{O} = 6.6 \times 10^{-10}$ m

The relationship between $N_{Cu\text{-}surf}$, $N_{Ce\text{-}surf}$, $N_{O\text{-}surf}$ was calculated based on XPS and relevant values were listed in Table S3.

1.3 normalized reaction rate

NO+CO reaction on the catalyst is recognized as a firstorder reaction with respect to NO. Assuming the diffusion to be limitation-free, the reaction rate (r) can be calculated using NO conversion below 20% as

$$r = -\frac{F \times \alpha}{S_{Mn-surf}}$$

where F is the flow of gaseous molecules (mol s^{-1}), α is the fractional conversion, and $S_{Mn\text{-}surf}$ is the surface area of Mn atoms on the surfaces of catalysts (m^2). $N_{Mn\text{-}surf}$ and $S_{Mn\text{-}surf}$ were estimated from the BET and XPS data as reported before[1].

1.4 Calculation of apparent activation energy (Ea)

The Arrhenius formula (k=A exp (Ea/RT)) was applied to calculate the apparent activation energies (Ea) from the slope of the linear plot of ln(R) versus 1000/T, and use it to analyze the difference in catalytic activity of CuO_x/CeO_2-X catalysts. Ea and k were calculated by the following equation:

$$k = -\frac{V}{w} \times \ln(1 - x)$$

$$\ln k = -\frac{Ea}{RT} + \ln A$$

k is the reaction rate constant (mol g^{-1} s^{-1}), V is the total gas flow (mol s^{-1}), w is the mass of catalyst (g), x is the NO conversion (%), Ea is the apparent activation energy of catalyst (kJ mol^{-1}), R is the gas constant (8.314 J mol^{-1} K^{-1}), T is the reaction temperature (K) and A is the pre-exponential factor (mol g^{-1} s^{-1}).

2 Figure captions

Fig. S1 The N_2 selectivity (%) of (a) CuO_x/CeO_2-H, (b) CuO_x/CeO_2-T, (c) CuO_x/CeO_2-C, (d) CuO_x/CeO_2-F at different GHSV.

Fig. S2 Resistance tests to $O_2 + H_2O + SO_2$ over CuO_x/CeO_2-H catalysts at 270 °C.

Fig. S3 XRD patterns of CeO_2-X.

Fig. S4 SEM images of CuO_x/CeO_2-H(a), CuO_x/CeO_2-T(b), CuO_x/CeO_2-C(c) and CuO_x/CeO_2-F(d).

Fig. S5 Raman spectra of CeO_2-X.

Fig. S6 N_2 adsorption/desorption isotherms (a) and pore size distribution (b) of CuO_x/CeO_2-X catalysts.

Fig. S7 S_{BET} normalized reaction rates of CuO_x/CeO_2-X catalysts for NO+CO reaction.

Fig. S8 In situ FTIR spectra of NO adsorption on sulfurized CuO_x/CeO_2-X at 150 °C.

Fig. S9 NO conversion in NO+CO reaction over the catalysts. Reaction conditions: [NO] = 350 ppm, [CO] = 700 ppm, GHSV=450,000 h^{-1}.

3 Table captions
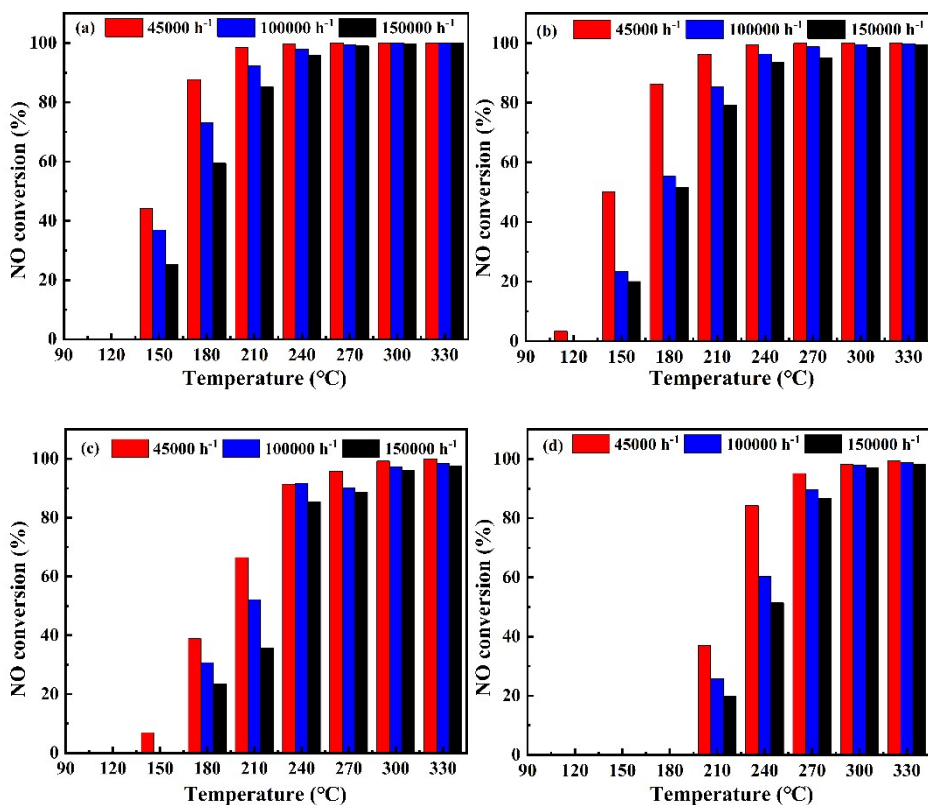
Table S1 Catalytic performance of transition metal oxide Reported in the

Literature.

Table S2 The surface areas, pore diameter, pore volume and lattice.

Table S3 TOF parameter information of CuO_x/CeO_2-H, CuO_x/CeO_2-T,

CuO_x/CeO_2-C(c) and CuO_x/CeO_2-F catalysts.
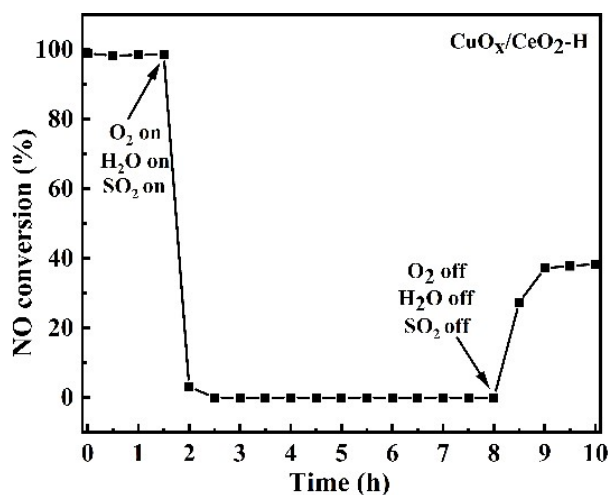
Figure:

Fig. S1 The N_2 selectivity (%) of (a) CuO_x/CeO_2-H, (b) CuO_x/CeO_2-T, (c) CuO_x/CeO_2-C, (d) CuO_x/CeO_2-F at different GHSV.
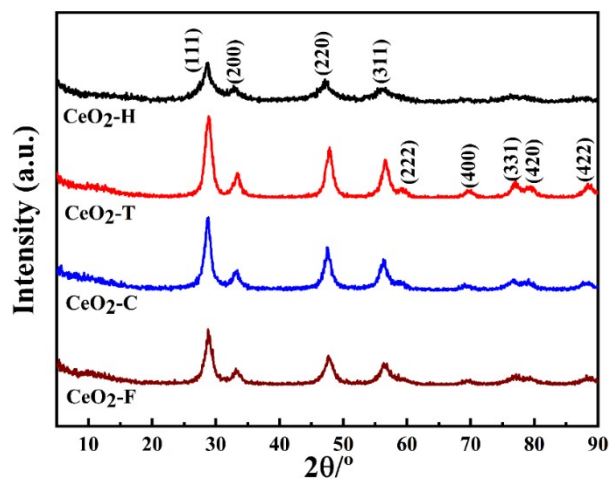

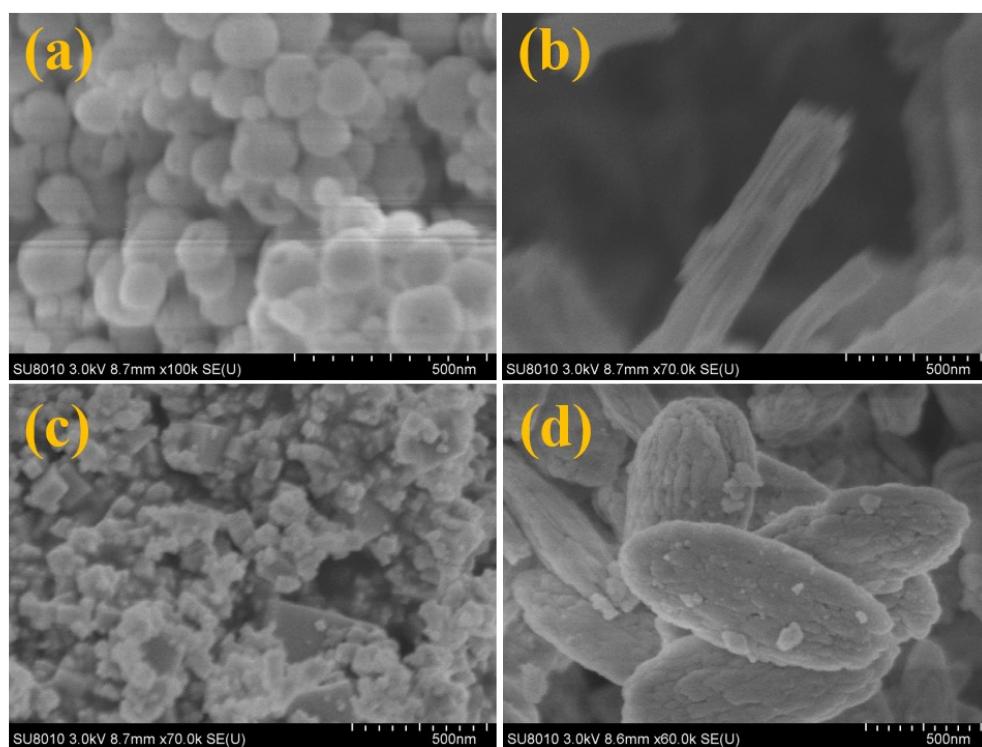**Fig. S2** Resistance tests to $O_2 + H_2O + SO_2$ over CuO_x/CeO_2-H catalysts at 270 °C.

1

2   **Fig S3** XRD patterns of CeO$_2$-X supports.

3

4   **Fig. S4** SEM images of CuO$_x$/CeO$_2$-H(a), CuO$_x$/CeO$_2$-T(b), CuO$_x$/CeO$_2$-C(c), and
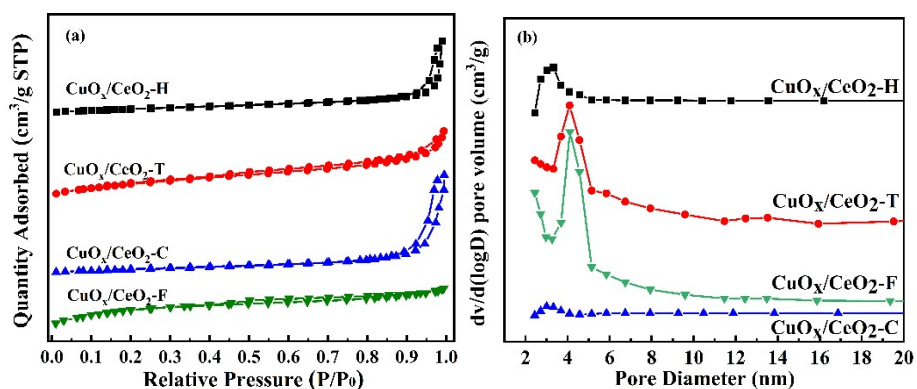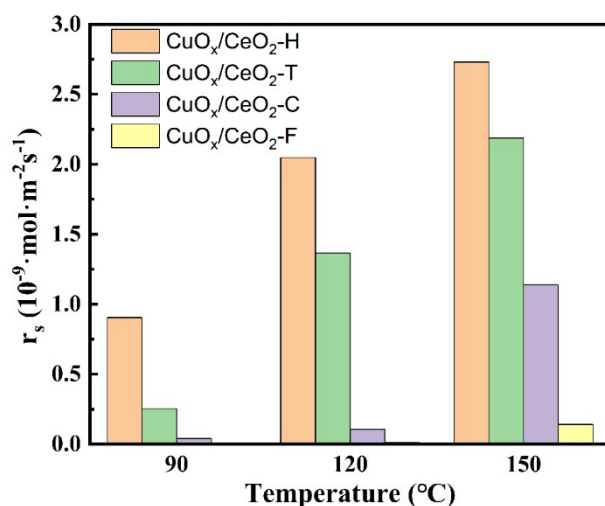5   CuO$_x$/CeO$_2$-F(d).
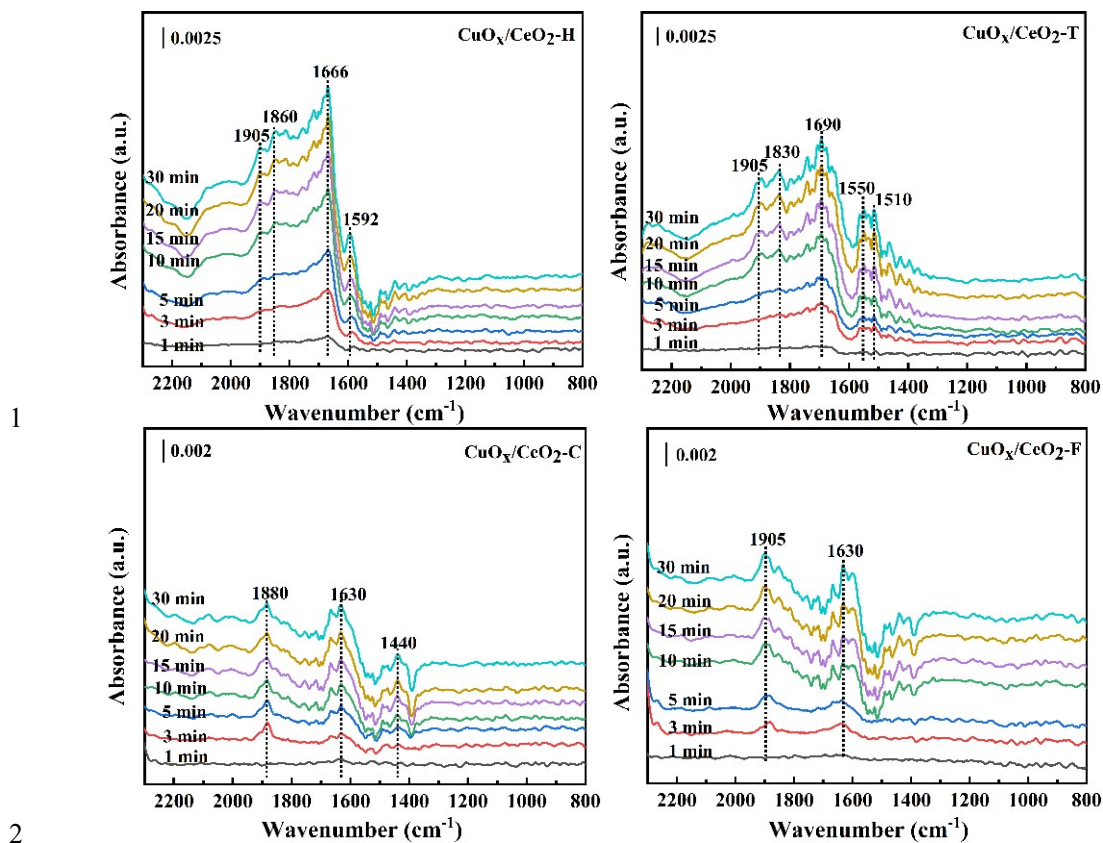
6

Fig. S5 Raman spectra of CeO_2-X.

Fig. S6 N_2 adsorption/desorption isotherms (a) and pore size distribution (b) of CuO_x/CeO_2-X catalysts.

Fig. S7 S_{BET} normalized reaction rates of CuO_x/CeO_2-X catalysts for NO+CO reaction.

Fig. S8 In situ FTIR spectra of NO adsorption on sulfurized CuO_x/CeO_2-X at 150 °C.
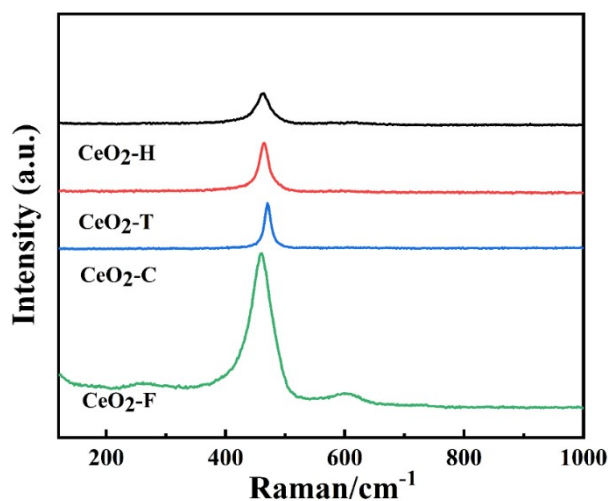
As shown in Fig. S8, the peaks located at 1860, 1905 cm^{-1} (CuO_x/CeO_2-H), 1830, 1905 cm^{-1} (CuO_x/CeO_2-T), 1880 cm^{-1} (CuO_x/CeO_2-C) and 1905 cm^{-1} (CuO_x/CeO_2-F) are attributed to the gaseous NO/ weak adsorption of NO on Cu^+ or Cu^{2+}. The bands located at 1666 cm^{-1} (CuO_x/CeO_2-H) and 1690 cm^{-1} (CuO_x/CeO_2-T) correspond to bridged nitrate. The peaks located at 1630 cm^{-1} (CuO_x/CeO_2-C, CuO_x/CeO_2-F) can be attributed to vibration modes of bridging bidentate nitrates [2-7]. The bands at 1592 cm^{-1} (CuO_x/CeO_2-H) and 1550 cm^{-1} (CuO_x/CeO_2-T) are coincided with the chelating bidentate nitrates. While two bands at 1510 cm^{-1} (CuO_x/CeO_2-T) and 1440 cm^{-1} (CuO_x/CeO_2-C) correspond to monodentate nitrates and linear monodentate nitrites, respectively. From Fig. S6, it is

discovered that the peak strength of CuO_x/CeO_2-H and CuO_x/CeO_2-T is slightly higher than that of CuO_x/CeO_2-C and CuO_x/CeO_2-F. The results indicate that CuO_x/CeO_2-H and CuO_x/CeO_2-T can effectively alleviate the competitive adsorption between NO and SO_2.
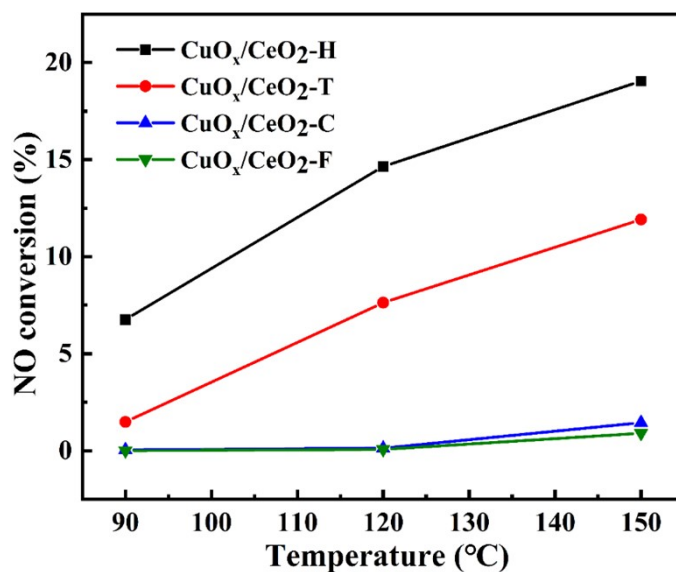
Fig. S9 NO conversion in NO+CO reaction over the catalysts.
Reaction conditions: [NO] = 350 ppm, [CO] = 700 ppm, GHSV=450,000 h^{-1}.

Table:

Table S1 Catalytic performance of transition metal oxide Reported in the Literature.

| Catalyst | Reaction conditions | | | | T_{50} | T_{max} | Ref. |
	Temperature range (°C)	GHSV or WHSV	NO (ppm)	CO (ppm)			
MnO_x/TiO_2	200	$50,000h^{-1}$	400	400	\	200	8
Cu-Ce/CNT	140-260	$12,600\ h^{-1}$	250	5000	170	240	9
$NiO-CeO_2$	100-300	$9000\ ml\ g^{-1}\ h^{-1}$	2.5%	5%	135	175	10
Fe/TiO_2	150–500	$75,000\ h^{-1}$	5000	5000	470	500	11
CuO/ZrO_2	100-450	$12,000\ h^{-1}$	5%	10%	250	450	12
Cu/TiO_2-CeO_2	150-400	$24,000\ ml\ g^{-1}\ h^{-1}$	5%	10%	220	310	13
CuO/CeO_2	100-200	$12,000\ h^{-1}$	5%	10%	\	200	14
Cu/CeO_2	100-325	$15,000\ ml\ g^{-1}\ h^{-1}$	5%	10%	135	300	15
CuO/CeO_2	100-330	$24,000\ ml\ g^{-1}\ h^{-1}$	5%	10%	175	300	16
CuO/CeO_2	100-400	$12,000\ ml\ g^{-1}\ h^{-1}$	5%	10%	150	400	17
Cu/CeO_2	150-400	$32,000\ h^{-1}$	5000	5000	\	300	18
CuO/CeO_2	50-300	$36,000\ ml\ g^{-1}\ h^{-1}$	1 vol%	1 vol%	105	200	19
CuO_x/CeO_2-H	90-330	$45,000\ h^{-1}$	350	700	102	270	This work

GHSV means gaseous hourly space velocity (h^{-1})

WHSV means weight hourly space velocity ($ml\ g^{-1}\ h^{-1}$)

T_{50} represents the temperature when the efficiency is 50%

T_{max} represents the temperature when the efficiency is maximum

1

Table S2 The surface areas, pore diameter, pore volume and lattice parameter of supports.

Catalysts	S_{BET} [a] (m²/g)	Pore diameter[b] (nm)	Pore volume[c] (cm³/g)	Lattice parameter (Å)
CeO$_2$-H	29	11	0.1	5.46
CeO$_2$-T	85	7	0.1	5.37
CeO$_2$-C	20	26	0.1	5.38
CeO$_2$-F	125	4	0.1	5.41

[a] Calculated by BET method [b,c] Calculated by BJH formula

5

Table S3 TOF parameter information of CuOx/CeO2-X catalysts.

Catalysts	Mass (g)	S_{BET} (m²·g⁻¹)	Normalized ratio of each element		
			Cu	Ce	O
CuO$_x$/CeO$_2$-H	0.04	112	1.00	2.84	10.27
CuO$_x$/CeO$_2$-T	0.04	84	1.00	3.50	11.37
CuO$_x$/CeO$_2$-C	0.04	19	1.00	1.74	6.49
CuO$_x$/CeO$_2$-F	0.04	92	1.00	2.66	10.65

7

References

1. C. Huang, Y. Zhu, X. Wang, X. Liu, J. Wang and T. Zhang, Journal of Catalysis, 2017, 347, 9-20.

2. X. Cheng, X. Zhang, D. Su, Z. Wang, J. Chang and C. Ma, Applied Catalysis B: Environmental, 2018, 239, 485-501.

3. X. Yao, Y. Xiong, W. Zou, L. Zhang, S. Wu, X. Dong, F. Gao, Y. Deng, C. Tang, Z. Chen, L. Dong and Y. Chen, Applied Catalysis B: Environmental, 2014, 144, 152-165.

4. X. Yao, F. Gao, Q. Yu, L. Qi, C. Tang, L. Dong and Y. Chen, Catalysis Science & Technology, 2013, 3.

5. J. Liu, X. Li, Q. Zhao, J. Ke, H. Xiao, X. Lv, S. Liu, M. Tadé and S. Wang, Applied Catalysis B: Environmental, 2017, 200, 297-308.

6. L. Li, L. Zhang, K. Ma, W. Zou, Y. Cao, Y. Xiong, C. Tang and L. Dong, Applied Catalysis B: Environmental, 2017, 207, 366-375.

7. X. Yao, R. Zhao, L. Chen, J. Du, C. Tao, F. Yang and L. Dong, Applied Catalysis B: Environmental, 2017, 208, 82-93.

8. T. Boningari, S. M. Pavani, P. R. Ettireddy, S. S. C. Chuang and P. G. Smirniotis, Molecular Catalysis, 2018, 451, 33-42.

9. Z. Gholami and G. Luo, Industrial & Engineering Chemistry Research, 2018, 57, 8871-8883.

10. C. Tang, B. Sun, J. Sun, X. Hong, Y. Deng, F. Gao and L. Dong, Catalysis Today, 2017, 281, 575-582.

11. C. A. Sierra-Pereira and E. A. Urquieta-González, Fuel, 2014, 118, 137-147.

12. Q. Yu, X. Yao, H. Zhang, F. Gao and L. Dong, Applied Catalysis A: General, 2012, 423-424, 42-51.

13. C. Deng, B. Li, L. Dong, F. Zhang, M. Fan, G. Jin, J. Gao, L. Gao, F. Zhang and X. Zhou, Physical Chemistry Chemical Physics : PCCP, 2015, 17.

14. G. Xianrui, L. Hao, L. Lichen, T. Changjin, G. Fei and D. Lin, Journal of Rare Earths, 2014, 32, 139-145.

15. L. Liu, Z. Yao, Y. Deng, F. Gao, B. Liu and L. Dong, ChemCatChem, 2011, 3, 978-989.

16. X. Yao, Q. Yu, Z. Ji, Y. Lv, Y. Cao, C. Tang, F. Gao, L. Dong and Y. Chen, Applied Catalysis B: Environmental, 2013, 130-131, 293-304.

17. L. Liu, J. Cai, L. Qi, Q. Yu, K. Sun, B. Liu, F. Gao, L. Dong and Y. Chen, Journal of Molecular Catalysis A: Chemical, 2010, 327, 1-11.

18. J. Chen, Y. Zhan, J. Zhu, C. Chen, X. Lin and Q. Zheng, Applied Catalysis A: General, 2010, 377, 121-127.

19. Q. Shi, Y. Wang, S. Guo, Z.-K. Han, N. Ta, G. Li, Baiker and Alfons, Catalysis Science & Technology, 2021, 11, 6543-6552.